Iranian Journal of Basic Medical Sciences
ijbms.mums.ac.ir

Bioinformatic analysis and characterization of the Anti-CD20 scFv-Conjugated Fe_3O_4 nanoparticles for targeted therapy of CD20+ leukemia cells

Shabnam Tavangarroosta [1], Mojgan Bandehpour [2, 3]*, Masoumeh Rajabibazl [4]*, Farhood Najafi [5], Sepideh Ghani [3], Mahmoud Hassani [1], Bahram Kazemi [3]

[1] Department of Molecular Medicine, School of Advanced Technologies in Medicine, Shahid Beheshti University of Medical Sciences, Tehran, Iran
[2] Department of Medical Biotechnology, School of Advanced Technologies in Medicine, Shahid Beheshti University of Medical Sciences, Tehran, Iran
[3] Cellular and Molecular Biology Research Center, Shahid Beheshti University of Medical Sciences, Tehran, Iran
[4] Department of Clinical Biochemistry, School of Medicine, Shahid Beheshti University of Medical Sciences, Tehran, Iran
[5] Department of Environmental Research, Institute for Color Science and Technology, Tehran, Iran

ARTICLE INFO

Article type:
Original

Article history:
Received: Apr 6, 2026
Accepted: May 30, 2026

Keywords:
Chronic lymphocytic leukemia (CLL)
Iron oxide nanoparticles
Molecular docking
ScFv antibody

ABSTRACT

Objective(s): Chronic lymphocytic leukemia (CLL) is one of the common types of leukemia. Various approaches for CLL therapy have been advanced, but they have some adverse effects. Iron oxide (Fe_3O_4) nanoparticles are promising drug carriers due to their magnetic properties and biocompatibility.

Materials and Methods: The recombinant anti-CD20 scFv was computationally modeled using the AlphaFold server. The complementarity-determining regions (CDR) of scFv were identified using the IMGT/V-Quest database. Molecular docking was performed separately between the scFv antibody and the CD20 antigen (ClusPro 2.0) and between Fe_3O_4 and the scFv (PyRx). Then, synthesized Fe_3O_4 nanoparticles were characterized using X-ray diffraction (XRD), field-emission scanning electron microscopy (FE-SEM), dynamic light scattering (DLS), and Fourier-transform infrared spectroscopy (FTIR). *In vitro* biological evaluation of the complexes was performed using the MTT assay.

Results: The molecular docking studies revealed favorable interactions between the recombinant scFv antibody and the CD20 antigen. Fe_3O_4 nanoparticles were included as a simplified ligand model to explore possible surface interaction patterns with the scFv molecule, suggesting no predicted interactions with CDR regions in the docking model. Physicochemical characterization confirmed the successful synthesis and desirable structural attributes of the Fe_3O_4 nanoparticles. In vitro biological evaluation of the Fe_3O_4 nanoparticle–anti-CD20 scFv complex revealed that cell death in the Raji cell line was significantly higher than in the control groups, underscoring the targeted cytotoxic efficacy.

Conclusion: The findings suggest that the Fe_3O_4 nanoparticle complex conjugated to an anti-CD20 scFv antibody can serve as a novel strategy for CLL treatment, contributing to the development of targeted therapies for cancer.

▶ Please cite this article as:
Tavangarroosta Sh, Bandehpour M, Rajabibazl M, Najafi F, Ghani S, Hassani M, Kazemi B. Bioinformatic analysis and characterization of the Anti-CD20 scFv-Conjugated Fe_3O_4 nanoparticles for targeted therapy of CD20+ leukemia cells . Iran J Basic Med Sci 2026; 29:

Introduction

One of the most common types of leukemia is chronic lymphocytic leukemia (CLL), which mostly affects the elderly. This disease is diagnosed by the accumulation of ineffective apoptosis-resistant B lymphocytes in the blood, bone marrow, and lymph nodes. Additionally, due to immunodeficiency, infections are a significant cause of death in patients with CLL (1, 2). Due to the adverse effects of common treatments (3-5), the need for new treatment strategies, including targeted and personalized approaches, has been highlighted to reduce toxicity, prevent treatment resistance, and increase efficacy (6-8). Monoclonal antibodies (mAbs) have been considered innovative approaches that have revolutionized the treatment of CLL. The studies have reported the use of mAbs alone or in combination with chemotherapy, which has led to improved patient survival (9, 10). However, mAbs face limitations in cancer treatment due to their large size and high production costs. The use of single-chain variable fragments (scFv), which exhibit better pharmacokinetic properties, can be a suitable alternative to monoclonal antibodies (mAbs) (11-13).

CD20 is a non-glycosylated surface protein expressed on the mature B lymphocytes. Ofatumumab, a fully human monoclonal antibody targeting the CD20 antigen, binds to

***Corresponding authors:** Mojgan Bandehpour. School of Advanced Technologies in Medicine, Shahid Beheshti University of Medical Sciences, Tehran, Iran, Cellular and Molecular Biology Research Center, Shahid Beheshti University of Medical Sciences, 1st floor, No.53, Ghobadian Street, Valie asr Street, Tehran, Iran. Tel: +98-21-8866139, Email: m.Bandehpour@sbmu.ac.ir, Bandehpour@gmail.com; Masoumeh Rajabibazl. Department of Clinical Biochemistry, Faculty of Medicine, Shahid Beheshti University of Medical Sciences, Tehran, Iran. Tel: +98-21-22432570 Email: rajabibazl_m@yahoo.com, Email: rajabi_m@sbmu.ac.ir

both the small and large extracellular loops of CD20 with high affinity, leading to potent complement-dependent cytotoxicity and apoptosis in CLL cells(14, 15). Additionally, a study demonstrated a specific and strong binding of the isolated scFv to the CD20 antigen (16). In recent years, tumor-targeted nanoparticles have shown great promise for cancer treatment, leading to improved efficacy (17). Fe_3O_4 nanoparticles (NPs) can be utilized for targeted drug delivery due to their biocompatibility, ease of functionalization, and ability to direct to specific sites (18, 19).

Combining the Fe_3O_4 nanoparticles with anti-CD20 scFv may improve the specificity and effectiveness of CLL treatments by enabling targeted delivery of therapeutic agents directly to malignant B cells.

This study aims to synthesize Fe_3O_4 nanoparticles functionalized with recombinant single-chain variable fragment (scFv) antibodies that target CD20. Their potential as a targeted therapy will be evaluated in Raji cells, a well-established model for CLL. By employing both in silico molecular docking studies and experimental evaluation, this research aims to elucidate the interactions between the nanoparticles, scFv, and the CD20 antigen. The findings from this investigation could pave the way for novel therapeutic strategies that utilize nanotechnology to achieve improved treatment outcomes in patients with CLL.

Materials and Methods

The following materials and equipment were used: FT-IR (Perkin-Elmer Spectrum One, Perkin-Elmer), High Performance XRD Diffractometer (Explorer - GNR Company, Italy), FE-SEM (TESCAN VEGA3, TESCAN), UV-Vis (Avaspec Dual, Avantes), ELISA reader (BioTek 100TS), 3-Glycidyloxypropyltrimethoxysilane (Merk), Ferrous chloride tetrahydrate ($FeCl_2.6H_2O$, Merk), and ferrous chloride tetrahydrate ($FeCl_2.4H_2O$, Merk). Additionally, hydrochloric acid fuming (Sigma-Aldrich), penicillin–streptomycin (Sigma-Aldrich), trypan blue (Sigma-Aldrich), dimethyl sulfoxide (DMSO, Sigma-Aldrich), and MTT (Sigma-Aldrich) were obtained from Sigma-Aldrich (USA). Polyacrylic acid AKN-40 (Asan Chem), Cell lines(Raji and Jurkat) were obtained from the Pasteur Institute of Iran (Tehran, Iran); RPMI 1640, glutamine, Hepes, fetal bovine serum (FBS), and penicillin–streptomycin were sourced from Gibco BRL (Life Technologies, Paisley, Scotland), and cell culture plates and Falcon tubes were procured from SPL Life Sciences.

Retrieval and preparation of 3D structure of Fe_3O_4, CD20 antigen and scFv

The three-dimensional structure of Fe_3O_4 was taken from ChemSpider in mol format and then converted into SDF format using Open Babel version 2.3.0. The three-dimensional crystal structure of the CD20 antigen (PDB ID: 1S8B) was obtained from the Protein Data Bank (www.rcsb.org). Structure preparation was performed by removing all components except the structure of interest using UCSF Chimera. The CD20-specific recombinant molecule was derived from our previous study (16). The scFv structure was predicted using the AlphaFold server. The quality and validity of the model were assessed using the Ramachandran plot (http://www.ebi.ac.uk). Also, the complementarity-determining regions (CDRs) of the antibody light and heavy chains were identified to determine the effect of Fe_3O_4 binding to the antibody on the antigen-antibody interaction using the IMGT/V-Quest database.

Molecular docking study

Molecular docking between the CD20 antigen and the scFv molecule was performed with the ClusPro 2.0 web server using default parameters. The best docking models were selected based on cluster size and energy levels. Next, potential interacting residues and possible interactions between the CD20 antigen and scFv were identified using the PDBsum program. To explore potential interactions of iron oxide with the antibody, Fe_3O_4 was used as a simplified representation of an iron oxide nanostructure. Docking of Fe_3O_4 with the scFv molecule was performed using AutoDock Vina in PyRx to investigate potential interactions. The results were qualitatively analyzed to assess whether iron oxide could interact with scFv surface regions. Chimera and PyMOL software were used to visualize the 3D structures and examine the intermolecular interactions **(20)**.

Synthesis of Fe_3O_4 nanoparticles (Fe_3O_4@P)

Briefly, 2.9 grams of $FeCl_3 \cdot 6H_2O$ and 1.1 grams of $FeCl_2 \cdot 4H_2O$ were placed in an Erlenmeyer flask and dissolved in 40 milliliters of ultrapure water. Then, the mixture was stirred at room temperature, yielding a clear, yellow solution. Separately, 5 grams of PAA (in liquid form, containing 50% water) were dissolved in 20 ml of water. After that, 2 milliliters of HCl (37%) were added to the PAA solution, which was then added to the Erlenmeyer flask containing iron salts, resulting in the solution turning cloudy yellow. Then, 4 grams of sodium hydroxide were dissolved in 56 milliliters of water, and the resulting solution was subsequently added to the salt solution, which was stirred at 100°C for 1 hour. As a result of the addition of Base due to oxidation, iron salts are formed, and the color of the reaction changes from cloudy yellow to black, with the oxidation process completing at elevated temperatures. After this period, 300 milliliters of water were added to the solution and placed on a strong magnet. After the solution separated into two phases, the black phase, containing the nanoparticles, was retained, while the upper solution, consisting of water and salts from the secondary reaction, was discarded. This process was repeated three to four times (Figure 1).

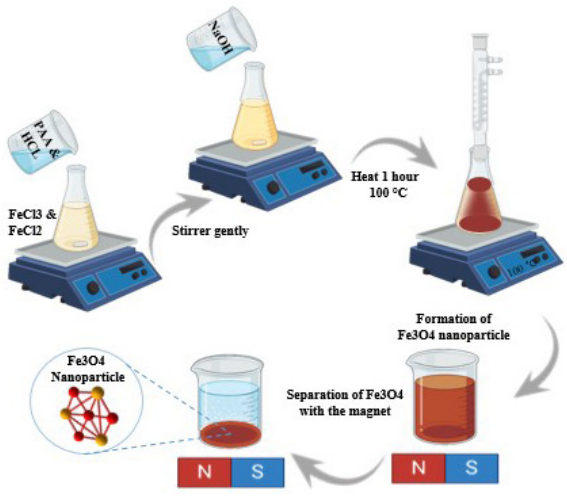

Figure 1. Stages of synthesizing Fe_3O_4 nanoparticles
Fe_3O_4: Iron oxide nanoparticles

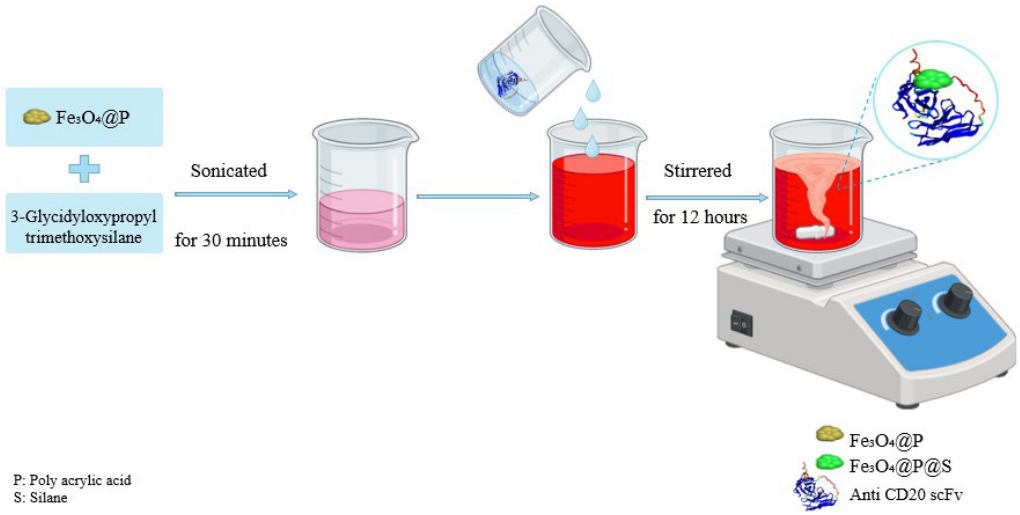

Figure 2. The figure schematically illustrates the process of attaching Fe_3O_4 to scFv
Fe_3O_4: Iron oxide nanoparticles; scFv: Single-chain fragment variable

Synthesis of Fe_3O_4 nanoparticles containing the chemical linker 3-glycidyloxypropyltrimethoxysilane (Fe_3O_4@P@S)

One gram of 3-chloropropyltrimethoxysilane was added to 9 grams of the Fe_3O_4@P sample. Subject the mixture to sonication using a sonic probe at 70 Hz, with each sonication cycle lasting 10 min and repeating three times. It was pulsed for 0.5 seconds within each cycle. After sonication, the sample was placed on a strong magnet. Once phase separation occurred, the black part containing the nanoparticles was retained, and the upper solution was discarded, which contained water and salts from the secondary reaction. The washing and phase separation process was repeated three to four times.

Connection of Fe_3O_4 nanoparticles to anti-CD20 scFv (Fe_3O_4@P@S@scFv)

The scFv recombinant protein against CD20, which had previously been studied by our team, was expressed and purified using the same protocols based on the author's previous published article (16). 100 micrograms of the nanoparticle Fe_3O_4@P@S were mixed with 200 micrograms of scFv that dissolved in ultrapure water. The mixture was gently stirred at room temperature for 12 hr to allow for efficient binding of the scFv to the nanoparticle surface. The mixture was then placed on a very strong magnet. After 1 hr, phase separation was performed, and the black part—containing nanoparticles bound to scFv—was kept. The upper solution, which contained unbound scFv, was analyzed to determine the concentration of protein that did not bind to the nanoparticles(Figure 2). This upper solution was analyzed for the loading capacity test.

Validation tests to prove the correct synthesis of Fe_3O_4 nanoparticles. (XRD, TEM, DLS, FTIR, UV-vis)

For confirmation of the synthesized nanoparticles, tests such as FE-SEM were conducted to measure particle size. The surface charges were measured using the Dynamic Light Scattering (DLS) technique, and UV-Vis and FT-IR spectroscopy were utilized for release analysis.

Infrared spectroscopy (FT-IR)

Each peak in the Infrared Spectroscopy indicates the level of absorption at the corresponding wavenumber, and the wavenumber of each peak signifies the presence of a specific functional group in the sample. Among the information that can be obtained are the identification and qualitative and quantitative determination of organic compounds containing nanoparticles as well as the determination of the type of functional groups and bonds present in their molecules. Additionally, this technique was used to confirm the attachment of the anti-CD20 scFv to the nanoparticle.

FE-SEM and DLS

To determine the size and morphology of Fe_3O_4 nanoparticles, a field emission scanning electron microscope was employed. Dynamic light scattering (DLS) analysis was performed to determine the hydrodynamic size and also the zeta potential of Fe_3O_4 nanoparticles using the Nano ZS model (ZEN 3600, Malvern Instruments).

X-ray diffraction(XRD)

The structural properties and crystal size of the synthesized Fe_3O_4 NPs were evaluated using X-ray diffraction analysis. XRD was used for analyzing the chemical components and determining the size and crystal structures. XRD undergoes specific steps, starting with the casting of a beam of X-rays on the crystals. The incident beam is then dispersed by the atoms, resulting in the emergence of diffraction patterns, followed by the interference of the beams with each other. This analysis was carried out with CuKa radiation (k=1.5406A° Å) with scanning in the range of 5–80_ for 2h angle. The crystal size (d) of the synthesized samples was calculated using the Scherrer equation. K is the Scherer constant (K = 0.89), b is the peak width at half maximum (radian), k is the X-ray wavelength (k = 1.5406 Å), and hr is the Bragg angle.

Ultraviolet-visible spectroscopy (UV-Vis)

The amount of light absorbed in a liquid is directly related to the concentration of that substance. The light was emitted using a tungsten lamp in the visible spectrophotometer (400-800 nm) and a deuterium lamp in the UV device (190-400 nm). After passing through the sample solution, the remaining light was detected by a sensor, and, after computer processing, it was displayed on the device's screen as a percentage of light transmittance and an absorbance value.

Determination of complex antibody loading capacity and conjugation efficiency

The free antibodies and nanoparticles were separated through a high-strength magnet. Briefly, 100 microliters of fresh nanoparticles were added to scFv Anti-CD20, stirred for 12 hr, and then placed on a strong magnet for 45 min. After incubation, the conjugated nanoparticles were separated from the supernatant using a strong magnetic field. The supernatant, containing unbound scFv, was collected. Then, the supernatant containing unbonded scFv was collected, and its concentration was determined by the Bradford assay. This measurement enabled the calculation of the protein loading capacity of the nanoparticle. The recovered black precipitate consisted of scFv-conjugated Fe_3O_4@PAA nanoparticles.

The Antibody loading Capacity (AbL) and Conjugation efficiency (CE) were calculated using the following equations:

$$CE\ (\%) = \frac{\text{total amount of Antibody} - \text{amount of unconjugated Antibody}}{\text{total amount of Antibody}} \times 100$$

$$AbL\ (\%) = \frac{\text{total amount of Antibody in nanoparticle total}}{\text{amount of nanoparticles}} \times 100$$

Examination of the toxicity of synthesized nanoparticle groups

Blood compatibility of the synthesized nanoparticles was assessed using an optimized hemolysis assay to measure the damage to the red blood cell membrane and hemoglobin release. Healthy human blood cells were collected, centrifuged, and the supernatant was replaced with PBS. The red blood cells (RBCs) were diluted 1:100 with cold PBS. PBS and Triton X-100 were used as negative and positive controls, respectively (21). Nanoparticles at varying concentrations (0, 12.5, 25, 50, 100, 200, 400, 600, 800, 1000 µg/ml) were added to diluted blood samples. Samples were incubated in a shaking incubator, then centrifuged and incubated at room temperature to separate non-lysed RBCs. Absorbance was measured at 405 nm, and the hemolysis percentage was calculated as follows:

$$\text{Hemolysis percentage} = \frac{\text{treated sample} - \text{negative control}}{\text{positive control} - \text{negative control}} \times 100$$

Examination of cell viability in Raji and Jurkat cell lines

To assess the cytotoxicity of the anti-CD20 single-chain antibody (scFv), iron oxide nanoparticles (IONPs), and scFv-conjugated IONPs, an MTT assay (22) was performed on Jurkat and Raji cell lines. Cells were seeded in 96-well plates at a density of 2.5×10^4 cells/well for Raji cells and 5×10^4 cells/well for Jurkat cells (in 100 µl of medium per well). After 24 hr of incubation at 37°C, cells were treated with the respective compounds. Following another 24-hour incubation period, 10 µl of MTT solution (5 mg/ml) was added to each well, and the plates were incubated for an additional 4 hr at 37°C. Subsequently, the medium was carefully removed, and 100 µl of dimethyl sulfoxide (DMSO) was added to each well to dissolve the formed formazan crystals. The absorbance was measured at 570 nm (reference wavelength 630 nm) using an ELISA reader. All procedures were conducted in accordance with standard protocols, and the results were analyzed using GraphPad Prism 8(One-way ANOVA).

Transfection of the Fe_3O_4@P@S@scFv complex to Raji and Jurkat cells

Raji (CD20+) and Jurkat (CD20-) human leukemia cell lines were cultured in RPMI supplemented with 10% FBS (Gibco, Invitrogen, Carlsbad, CA) and 100 units/ml penicillin and 100 µg/ml streptomycin. The cells were incubated for 24 hr at 37 °C in 5% CO_2 until they reached 80–90% confluency. After that, the experiments were conducted.

Statistical analysis

Statistical analysis was conducted using GraphPad Prism 8. Results are shown as mean ± standard deviation. One-way ANOVA was used, with *P*-values less than 0.05 (*), 0.01 (**), 0.001 (***), and 0.0001 (****) considered statistically significant; a single asterisk (*) indicates $P<0.05$, two (**) indicate $P<0.01$, three (***) indicate $P<0.001$, and four (****) indicate $P<0.0001$. Each experiment was performed at least three times.

Results

Prediction and evaluation of the 3D structure of scFv

AlphaFold2 can predict 3D structures and assess their accuracy using pLDDT and pTM scores. In this research, the scFv model was chosen based on a pLDDT score of 89.9 and a pTM score of 0.85, indicating a high- confidence model. Furthermore, the evaluation results of the three-dimensional model, as indicated by the Ramachandran plot, showed that 90.0% of the residues are in the favored regions (Figure 1 in the Supplementary). Also, the CDR regions determined by IMGT/V-Quest are shown in Figure 2 in the Supplementary.

CDR regions of the scFv anti- CD20

While CDR3 was highly conserved, noticeable differences in the boundaries of CDR1 and CDR2 were evident among schemes. The additional residues identified in the Kabat, Chothia, and Contact definition are likely to affect antigen-binding geometry. These findings highlight that framework-dependent CDR definitions can affect structural modeling and functional prediction of antibody–antigen interactions (Figure 2 in the Supplementary).

Molecular docking

Molecular docking of CD20 antigen with scFv was performed using ClusPro 2.0 server, and the best model with the lowest energy was selected. The residues involved in this interaction were identified using the PDBsum program (Figure 3a, b). Also, the molecular docking results showed that the CD20 antigen forms 7 hydrogen bonds with the light chain and 3 with the heavy chain of the scFv. Additionally, the results demonstrated the formation of a salt bridge between the antigen and the scFv light chain. Also, the three-dimensional structure of the docking complex of the CD20 antigen with scFv was displayed using Chimera (Figure 3C).

In addition, molecular docking studies were performed using PyRx to identify and assess the interactions and binding affinity between scFv and Fe_3O_4. The results revealed a binding free energy of -4.6 kcal/mol, indicating the stability of the Fe_3O_4-scFv complex. The 3D structure visualization of the CD20 antigen-antibody-Fe_3O_4 docking complex was performed using PyMOL software (Figure 3 in the Supplementary), which showed the formation of three hydrogen bonds between Fe_3O_4 and the residues Tyr214, Tyr213, and Gly215 in the heavy chain.

Confirmation of the synthesis of Fe_3O_4 nanoparticles

Infrared spectroscopy (FT-IR)

The FT-IR spectrum of the nanoparticles (Fe_3O_4@PAA, Fe_3O_4@PAA@S, Fe_3O_4@PAA@S@scFv) was compared,

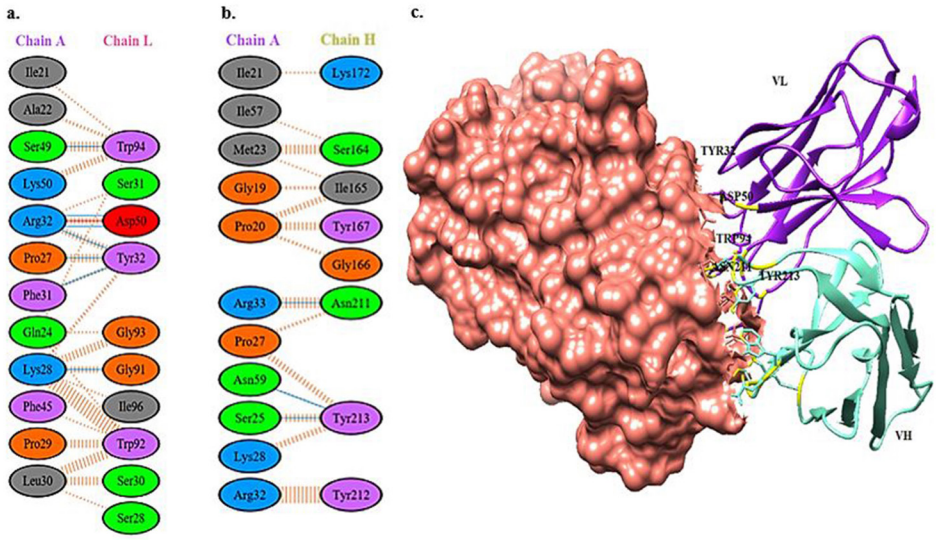

Figure 3. Three-dimensional structure of the antigen–antibody complex
a. Schematic representation illustrating hydrogen bonds and hydrophobic interactions between residues of Chain A (antigen) and Chain L.b. Interaction map highlighting the principal residues at the binding interface between Chain A(antigen) and Chain H. c. The variable light (VL, purple) and variable heavy (VH, cyan) domains bound to the antigen surface (visualized using Chimera).

and the results confirmed the successful synthesis of the nanoparticles (Figure 6). The FTIR spectrum of Fe_3O_4@P reveals characteristic absorption peaks at approximately 3382 and 2932 cm^{-1}, corresponding to O–H and C–H stretching vibrations, respectively. The peaks at 1708 and 1405 cm^{-1} indicate the presence of carboxylic acid groups (C=O and C–O), originating from polyacrylic acid (PAA) coating. Furthermore, Fe–O stretching vibrations are evident at ~630 and 585 cm^{-1}, confirming the retention of the magnetite core structure.

Following silanization, the FTIR spectrum of Fe_3O_4@P@S displays new absorption bands at 1149 and 1074 cm^{-1}, attributed to Si–O–Si and Si–O–C vibrations, respectively. These signals confirm successful modification of the nanoparticle surface with a silane coupling agent.

Upon conjugation with scFv, the FTIR spectrum of Fe_3O_4@P@S@scFv exhibits additional peaks at 1658 and 1540 cm^{-1}, corresponding to amide I (C=O stretching) and amide II (N–H bending) vibrations. These are characteristic of peptide bonds and indicate the presence of protein molecules on the surface. Additionally, broadening and intensity changes in the 3300–3400 cm^{-1} region, attributed to N–H stretching, further confirm the immobilization of scFv.

Comparatively, the FTIR spectrum of pure scFv exhibits similar amide I and II bands at 1652 and 1542 cm^{-1}, along with N–H and C–H stretching at 3306, 2931, and 2852 cm^{-1}. The retention of amide bands in the spectrum of the final nanoconjugate (Fe_3O_4@P@S@scFv), along with unchanged Fe–O and silane-related bands, suggests that the bioconjugation was successful and did not compromise the structural integrity of either the protein or the magnetic nanoparticle (Figure 4).

Field emission scanning electron microscopy (FE-SEM)

The morphology of the nanoparticles Fe_3O_4@PAA, Fe_3O_4@PAA@S, and Fe_3O_4@PAA@S@scFv was examined using a Field

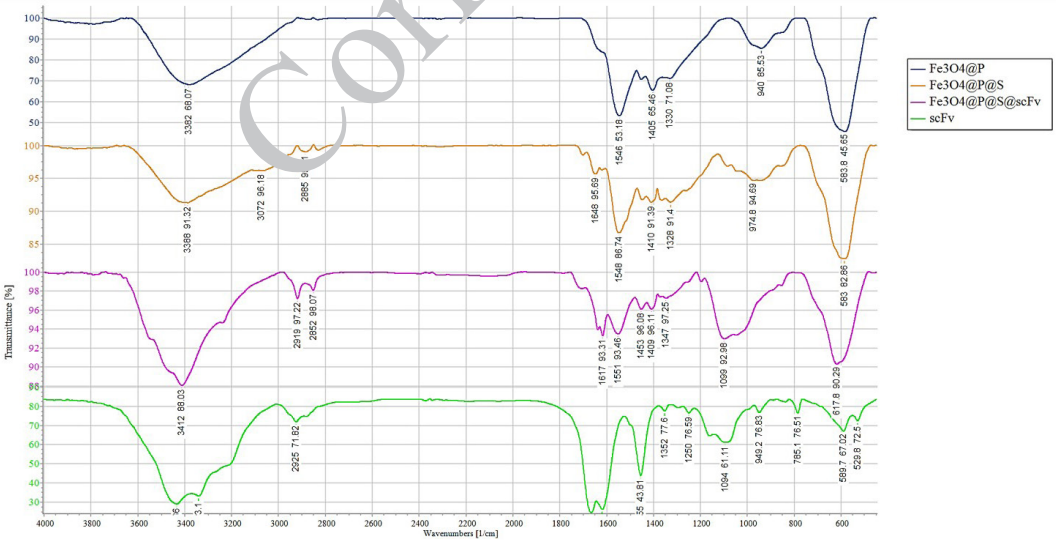

Figure 4. Peaks related to the samples Fe_3O_4@P, Fe_3O_4@P@S, scFv, and the sample Fe_3O_4@P@S@scFv are shown
SpectraGryph 1.2.15 - spectroscopy software used for FTIR analysis.
FTIR: Fourier transform infrared spectroscopy; Fe_3O_4: Iron oxide nanoparticles

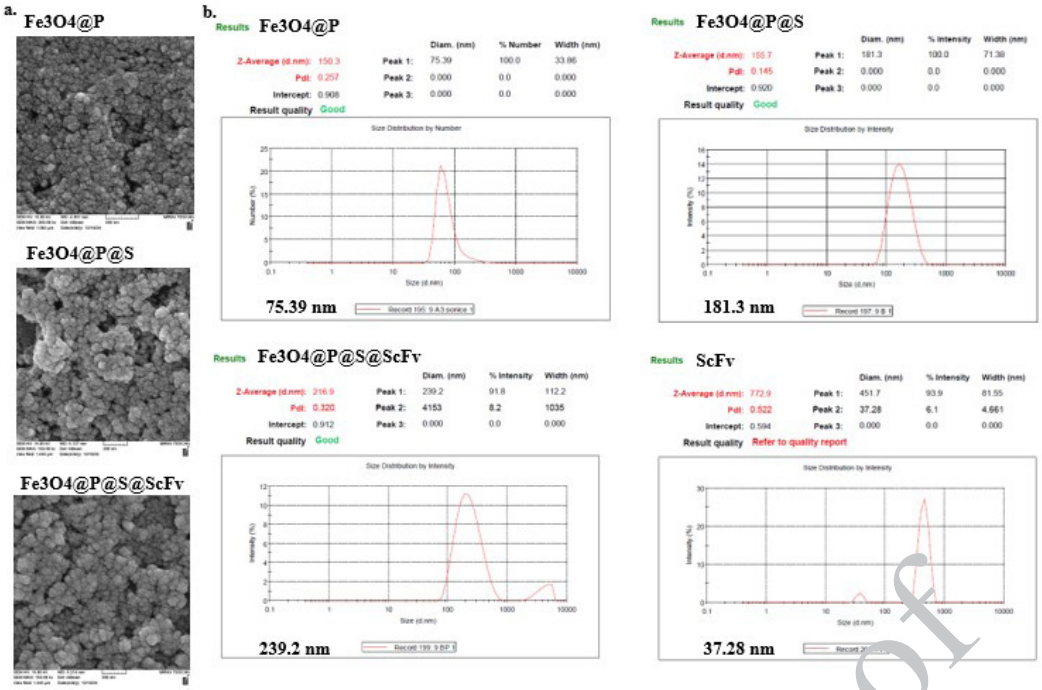

Figure 5. a Field emission scanning electron microscopy (FE-SEM) images of Fe_3O_4@PAA, Fe_3O_4@PAA@S, and Fe_3O_4@PAA@S@scFv nanoparticles
All nanoparticles exhibited a spherical and homogeneous morphology with smooth surfaces. A noticeable increase in particle size was observed after conjugation of scFv to Fe_3O_4@PAA@S, confirming the successful surface functionalization of nanoparticles with the antibody fragment. The average hydrodynamic size of the nanoparticles Fe_3O_4@P, Fe_3O_4@P@S, Fe_3O_4@P@S@scFv are 75.39, 181.3, and 239.2 nanometers, respectively, and scFv is 37.28 nm.
Fe_3O_4: Iron oxide nanoparticles; scFv: Single-chain fragment variable

emission scanning electron microscope. All the nanoparticles exhibited spherical and uniform shapes. In addition, FE-SEM analysis showed that the size of Fe_3O_4@PAA@S@scFv was larger than that of Fe_3O_4@PAA@S. These observations indicate that integrating scFv with Fe_3O_4@PAA@S has increased nanoparticle size, as shown in Figure 5. a.

Hydrodynamic size and zeta potential of nanoparticles

The average hydrodynamic size of the nanoparticles Fe_3O_4@P, Fe_3O_4@P@S, Fe_3O_4@P@S@scFv is, respectively, 75.39, 181.3, 239.2 nm. The scFv size was 37.28 nm. The zeta potential results from DLS were Fe_3O_4@P, Fe_3O_4@P@S, Fe_3O_4@P@S@scFv of: -14.8, -14.2, -29.2 mV. The scFv zeta potential was -16.7 mV. The difference in size and zeta potential among the nanocarriers was statistically significant. Ultimately, the polydispersity index (PDI) for the nanocarriers was in a good range. The average hydrodynamic size (Figure 5b) and zeta potential (Figure 4 in the Supplementary).

Characterization of the complexes

X-ray diffraction (XRD) of Fe_3O_4@P nanoparticle

The X-ray diffraction (XRD) pattern of the Fe_3O_4@PAA nanocomposite, recorded in the 2θ range of 20°–90°, is presented in Figure 6. The pattern reveals several distinct diffraction peaks, indicating the sample's crystalline nature. The main diffraction peaks appear at approximately 2θ values of 30.2°, 35.5°, 43.2°, 53.5°, 57.0°, and 62.6°, which correspond to the (220), (311), (400), (422), (511), and (440) crystal planes of magnetite (Fe_3O_4), respectively. These values are in good agreement with the standard JCPDS card No. 19-0629 for the spinel structure of Fe_3O_4. The most intense peak is observed at 2θ ≈ 35.5°, which is indexed to the (311) plane (Figure 6).

To further illustrate these results, the calculated interplanar spacings (d-values) using Bragg's law are summarized along with the corresponding Miller indices in Table 1.

Ultraviolet-visible spectroscopy (UV-Vis)

Figure 7 presents the UV–Vis absorbance spectra

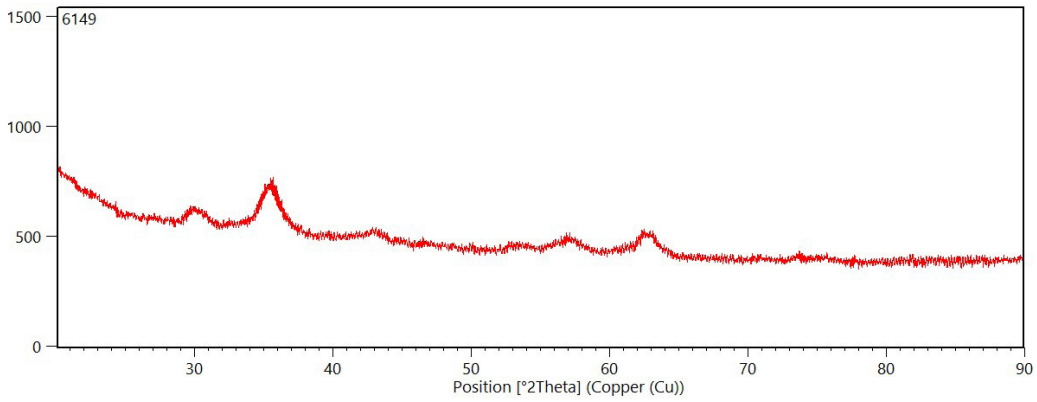

Figure 6. XRD pattern of the synthesized Fe_3O_4@PAA nanoparticle showing characteristic diffraction peaks corresponding to the spinel structure of Fe_3O_4
XRD: X-ray diffraction; Fe_3O_4: Iron oxide nanoparticles

Table 1. X-ray diffraction (XRD) data showing the main diffraction peaks, corresponding interplanar spacings (d-spacing), and Miller indices (hkl) of the crystalline planes

2θ (°)	d-spacing (Å)	Miller indices (hkl)
~30.2	2.96	(220)
~35.5	2.52	(311)
~43.2	2.09	(400)
~53.5	1.71	(422)
~57.0	1.61	(511)
~62.6	1.48	(440)

of Fe_3O_4@P (red curve), Fe_3O_4@P@S (yellow curve), Fe_3O_4@P@S@scFv (green curve), and free scFv (purple curve) in the wavelength range of 200–700 nm. All of the nanocomposite formulations exhibit strong absorbance in the ultraviolet region, particularly between 200 and 400 nm. The Fe_3O_4@P sample exhibits a broad absorption band centered at approximately 300 nm, which shifts slightly and increases in intensity upon subsequent surface functionalization.

The Fe_3O_4@P@S sample displays a broader, more intense absorbance profile than Fe_3O_4@P, indicating successful modification. After conjugation with scFv, the Fe_3O_4@P@S@scFv spectrum shows an additional absorbance shoulder near 280 nm, commonly associated with aromatic amino acids in proteins. The free scFv sample (purple curve) also exhibits a sharp peak around 280 nm, further confirming this characteristic absorption. Analysis revealed that Fe_3O_4@P, Fe_3O_4@P@S, and Fe_3O_4@P@S@scFv samples exhibited maximum absorbance (λ_max) at approximately 279 nm, 278.8 nm, and 222 nm, respectively. Additionally, free scFv displayed a maximum absorbance at 2[illegible] nm. The observed decrease in λ_max after scFv conjugation to Fe_3O_4@P@S, forming Fe_3O_4@P@S@scFv, can be attributed to a blueshift, which indicates changes in the electronic environment upon bioconjugation (Figure 7).

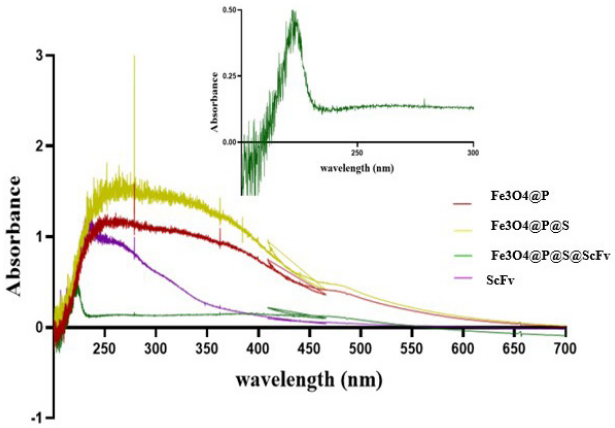

Figure 7. UV peaks related to the samples Fe_3O_4@P, Fe_3O_4@P@S, scFv, and the sample Fe_3O_4@P@S@scFv are shown
Fe_3O_4: Iron oxide nanoparticles; scFv: Single-chain fragment variable

Antibody loading capacity and conjugation efficiency of Anti-CD20 scFv to Fe_3O_4@P@S nanoparticles

To evaluate the optimal ratio for conjugating anti-CD20 scFv to Fe_3O_4@P@S nanoparticles, various scFv-to-nanoparticle feed ratios (1:1 to 1:20) were investigated. As shown in Table 2, the antibody loading capacity increased with higher scFv input, reaching a maximum of 78.0% at a 1:20 ratio. In contrast, the binding efficiency exhibited an inverse trend, decreasing from 55.0% at a 1:1 ratio to only 3.9% at the 1:20 ratio. Specifically, loading capacities of 55.0%, 42.7%, 62.3%, and 78.0% were observed for scFv ratios of 1, 5, 10, and 20, respectively, while the corresponding binding efficiencies were 55.0%, 8.5%, 6.2%, and 3.9%. Together, these results indicate that although increasing the amount of scFv in the reaction mixture enhances overall loading onto the nanoparticle surface, a significant portion remains unbound at higher feed ratios, thereby reducing conjugation efficiency. Therefore, the 1:1 ratio demonstrated the highest binding efficiency and is therefore suggested as the most efficient condition in terms of reagent utilization (Table 2).

Cytotoxicity assessment of Fe_3O_4-based nanoconstructs on Raji cells

The cytotoxic potential of Fe_3O_4-based nanostructures was examined in $CD20^+$ Raji cells using the MTT assay after 24 hr incubation at concentrations of 12.5–600 µg/ml (Figure 8a). All formulations induced a concentration-dependent decrease in cell viability relative to the untreated control (CTRL).

Fe_3O_4@P nanoparticles showed a moderate reduction in viability, with significant cytotoxicity observed at concentrations above 50 µg/ml (P<0.05). Fe_3O_4@P@S nanoparticles exhibited stronger cytotoxic effects, reducing cell viability to below 50% at 400–600 µg/ml (P<0.01).

Remarkably, conjugation of the anti-CD20 scFv to the Fe_3O_4@P@S surface (Fe_3O_4@P@S@scFv) resulted in enhanced cytotoxicity compared to the non-targeted formulations. Significant decreases in viability were observed from 50 µg/ml onward (P<0.05), reaching approximately 40% at 600 µg/ml (P<0.01). This effect can be attributed to the specific binding of the anti-CD20 scFv to its cognate receptor

Table 2. Antibody loading (AbL) and Conjugation efficiency (CE) of Fe_3O_4@P@S nanoparticles at different Anti-CD20 scFv concentrations
Increasing the scFv ratio enhanced loading efficiency but decreased overall encapsulation yield, indicating saturation of binding sites at higher antibody concentrations

Fe_3O_4@P@S (Ratio)	Anti-CD20 scFv (µg/ml)	DL (%)	EE (%)
1	1	55.0	55.0
1	5	42.7	8.54
1	10	62.3	6.23
1	20	78.0	3.90

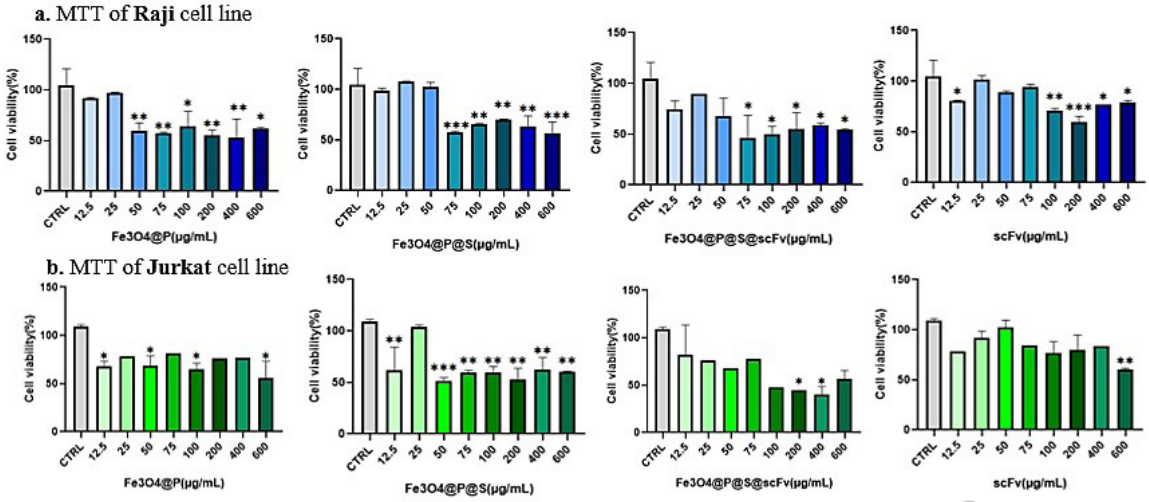

Figure 8. a. Raji ($CD20^+$) cells: MTT assay showed a dose-dependent decrease in cell viability after 24 hr treatment with Fe_3O_4@P, Fe_3O_4@P@S, Fe_3O_4@P@S@scFv, and free scFv. Fe_3O_4@P@S@scFv induced the strongest cytotoxic effect, attributed to specific anti-CD20 scFv binding, receptor-mediated internalization, and enhanced intracellular nanoparticle accumulation. b. Jurkat ($CD20^-$) cells: All formulations reduced cell viability dose-dependently after 24 hr. Fe_3O_4@P@S showed the highest nonspecific toxicity, while scFv conjugation reduced cytotoxicity, indicating improved biocompatibility without receptor-mediated targeting

scFv: Single-chain variable fragment; Fe_3O_4: Iron oxide nanoparticles; MTT: 3-(4,5-Dimethylthiazol-2-yl)-2,5-Diphenyltetrazolium bromide

on Raji cells, promoting receptor-mediated nanoparticle uptake and increasing intracellular accumulation.

Treatment with the free scFv alone also reduced viability at higher concentrations (≥100 μg/ml), suggesting partial receptor interaction, but its effect was less pronounced than that of the scFv-conjugated nanoparticles.

Overall, these results demonstrate that the Fe_3O_4@P@S@scFv nanoconstruct exhibits significant and selective cytotoxicity against $CD20^+$ Raji cells, confirming the role of scFv functionalization in facilitating targeted cellular interactions and enhancing therapeutic efficacy.

Cytotoxicity assessment of Fe_3O_4-based nanoconstructs on Jurkat cells

The cytotoxic effects of the synthesized Fe_3O_4-based nanostructures were evaluated in Jurkat cells using the MTT assay after 24 hr incubation at concentrations ranging from 12.5 to 600 μg/ml (Figure 8). A concentration-dependent reduction in cell viability was observed in all nanoparticle-treated groups compared to the untreated control (CTRL).

Fe_3O_4@P nanoparticles exhibited moderate cytotoxicity, with cell viability decreasing to approximately 60–70% at 600 μg/ml ($P<0.05$). The Fe_3O_4@P@S formulation showed markedly higher cytotoxicity, with significant decreases in viability even at 25 μg/ml ($P<0.01$) and further reductions to below 50% at higher concentrations, indicating strong dose-dependent toxicity.

Interestingly, the Fe_3O_4@P@S@scFv construct exhibited slightly lower cytotoxicity than Fe_3O_4@P@S, maintaining approximately 55–65% viability at concentrations above 100 μg/ml. Since Jurkat cells do not express CD20, the target antigen for this scFv, this reduction in toxicity likely reflects improved surface biocompatibility and shielding effects of the conjugated antibody fragment rather than receptor-mediated targeting. Treatment with the free scFv alone did not show significant cytotoxicity at most concentrations, with only the highest dose (600 μg/ml) producing a notable decrease in viability ($P<0.01$) (Figure 8b).

Collectively, these data demonstrate that while Fe_3O_4@P@S exhibits the strongest cytotoxic effect on Jurkat cells, conjugation with the anti-CD20 scFv attenuates nonspecific toxicity, indicating that surface functionalization can modulate nanoparticle–cell interactions even in non-target cell lines.

Discussion

$CD20^+$ B lymphocytes grow clonally in CLL. The way the illness reacts to conventional therapies is greatly influenced by these cells. In this research, we conjugated anti-CD20 single-chain variable fragment (scFv) antibodies to Fe_3O_4 magnetic nanoparticles to achieve more accurate targeting. With this method, a targeted nanoplatform is developed to enable more efficient delivery.

The Fe_3O_4 delivery system demonstrated notable stability, functionality, and biocompatibility, supporting its potential as a safe and efficient platform for targeted therapy against $CD20^+$ leukemia cells. This conclusion was based on comprehensive physicochemical characterization, including particle size distribution, zeta potential, morphology, structural integrity, and rigorous hemocompatibility testing to confirm clinical safety. A comprehensive set of *in vitro* experiments was conducted to evaluate the therapeutic potential of the Fe_3O_4–anti-CD20 scFv nanocomplex.

Recombinant anti-CD20 scFv exhibits a favorable binding affinity to the CD20 antigen, predicted through molecular docking analysis, which demonstrates specific interactions via hydrogen bonds and a salt bridge. Notably, interaction with Fe_3O_4 nanoparticles preserves the CDRs, thereby enabling continued antigen recognition. This supports prior findings that surface-functionalized nanoparticles can maintain antibody-binding activity with appropriate conjugation methods (23, 24). The use of AlphaFold2 to model the scFv structure and identify CDR regions yielded a reliable structural model, which was subsequently used for molecular docking (25, 26).

Physicochemical characterization: FE-SEM, DLS, and XRD analyses confirmed that the synthesized Fe_3O_4 nanoparticles were spherical, monodisperse, and crystalline. Functionalization with 3-Glycidyloxypropyltrimethoxysilane and subsequent conjugation with scFv increased particle size

and negative surface charge, which is consistent with other studies indicating that protein immobilization increases hydrodynamic diameter and alters zeta potential (27, 28). FTIR spectra further confirmed successful attachment of scFv to the nanoparticle surface without disrupting the core magnetite structure. These findings align with previous work showing that Fe_3O_4 nanoparticles conjugated to targeting moieties can maintain structural stability while retaining functional activity (29).

Targeted cytotoxicity: The MTT assay revealed that Fe_3O_4@P@S@scFv complex exhibited significantly enhanced cytotoxicity against Raji cells ($CD20^+$) compared to both free scFv and unfunctionalized nanoparticles, while Jurkat cells ($CD20^-$) were largely unaffected. This confirms the specificity of the scFv-conjugated nanoparticles and their potential to reduce off-target effects—a major limitation of conventional chemotherapy. Notably, the increased cytotoxicity at low concentrations indicates efficient cellular uptake via antigen-mediated endocytosis, consistent with previous studies demonstrating that antibody-functionalized nanoparticles enhance targeted delivery and therapeutic efficacy (30, 31).

The use of scFv fragments overcomes these limitations, offering a smaller size, better tumor penetration, and reduced immunogenicity. When scFv fragments are combined with Fe_3O_4 nanoparticles, the therapeutic potential is further enhanced by targeted delivery, potentially allowing dose reduction and minimizing systemic toxicity. Recent studies have also reported successful functionalization of magnetic nanoparticles with other antibody fragments, such as anti-EGFR scFv, demonstrating comparable improvements in target specificity and cytotoxicity (32). Our findings extend this strategy to $CD20^+$ CLL cells, providing a promising platform for clinical translation.

Conclusion

Although the current study provides a comprehensive *in vitro* evaluation, *in vivo* studies are necessary to assess pharmacokinetics, biodistribution, and therapeutic efficacy. Furthermore, optimization of nanoparticle surface chemistry may improve circulation time and reduce potential opsonization. Integration with additional therapeutic agents or combination therapy could further enhance anti-CLL activity.

In conclusion, our study demonstrates that Fe_3O_4 nanoparticles conjugated with anti-CD20 scFv are promising candidates for targeted CLL therapy, combining biocompatibility, specificity, and potent cytotoxicity. This work lays the foundation for developing next-generation nanomedicine platforms for hematological malignancies.

Acknowledgment

We thank the staff at the Cellular and Molecular Biology Research Center at Shahid Beheshti University of Medical Sciences, Iran, for their support. The results presented in this paper were part of Shabnam Tavangarroosta's Ph.D thesis.

Funding

This work was funded by grant number 43005986 .

Ethics Approval

The study adhered to ethical principles approved by the Medical Ethics Committee of Shahid Beheshti University of Medical Sciences (Code of Ethics: IR.SBMU.RETECH.REC.1402.386).

Authors' Contributions

M B and S T conceived and designed the project; S T, M B, and M H curated the data; S T, M B, and M H conducted the analysis; M B secured the funding; S T investigated; M B, M R, B K, and F N developed the methodology; M B and M R supervised the thesis; M B and B K validated the data; S T visualized the data; S T authored the original draft; M B, B K, and F N reviewed and edited the draft.

Conflicts of Interest

All authors of this article stated that they have no conflicts of interest.

Declaration

The authors declare no competing interests. We have used Grammarly to correct grammar in the manuscript. Figures in this paper were created using BioRender.com. Grammar editing and refinement were performed using ChatGPT. SpectraGryph 1.2.15 was used for FTIR analysis. HighScore Plus was used for XRD analysis.

References

1. Wainman LM, Kaur WA, Kaur P. Chronic lymphocytic leukemia: Current knowledge and future advances in cytogenomic testing. Exon Publications 2023:93-106.
2. Langerbeins P, Eichhorst B. Immune dysfunction in patients with chronic lymphocytic leukemia and challenges during COVID-19 pandemic. Acta Haematol 2021; 144:508-518.
3. Freifeld AG, Bow EJ, Sepkowitz KA, Boeckh MJ, Ito JI, Mullen CA, *et al.* Clinical practice guideline for the use of antimicrobial agents in neutropenic patients with cancer: 2010 update by the Infectious Diseases Society of America. Clin Infect Dis 2011; 52:e56-e93.
4. Friedman DL, Whitton J, Leisenring W, Mertens AC, Hammond S, Stovall M, *et al.* Subsequent neoplasms in 5-year survivors of childhood cancer: The childhood cancer survivor study. JNCI: J Natl Cancer Inst 2010; 102:1083-1095.
5. Howard SC, Trifilio S, Gregory TK, Baxter N, McBride A. Tumor lysis syndrome in the era of novel and targeted agents in patients with hematologic malignancies: A systematic review. Ann Hematol Oncol 2016; 95:563-573.
6. Iyer P, Wang L. Emerging therapies in CLL in the era of precision medicine. Cancers 2023; 15:1583.
7. Fatima N, Crassini KR, Thurgood L, Shen Y, Christopherson RI, Kuss B, *et al.* Therapeutic approaches and drug-resistance in chronic lymphocytic leukaemia. Cancer Drug Resist 2020; 3:532.
8. Woyach JA, Johnson AJ. Targeted therapies in CLL: Mechanisms of resistance and strategies for management. Blood 2015; 126:471-477.
9. Gezehagn Kussia G, Tessema TS. The potential of single-chain variable fragment antibody: Role in future therapeutic and diagnostic biologics. J Immunol Res 2024; 2024:1804038.
10. Ghani S, Bandehpour M, Yarian F, Baghaei K, Kazemi B. Production of a ribosome-displayed mouse scFv antibody against CD133, analysis of its molecular docking, and molecular dynamic simulations of their interactions. Appl Biochem Biotechnol 2024; 196:1399-1418.
11. Dabkowska A, Domka K, Firczuk M. Advancements in cancer immunotherapies targeting CD20: From pioneering monoclonal antibodies to chimeric antigen receptor-modified T cells. Front Immunol 2024; 15:1363102.
12. Pavlasova G, Mraz M. The regulation and function of CD20: An "enigma" of B-cell biology and targeted therapy. Haematologica 2020; 105:1494-1506.

13. Ho K-W, Chen I-J, Cheng Y-A, Liao T-Y, Liu E-S, Chen H-J, *et al.* Double attack strategy for leukemia using a pre-targeting bispecific antibody (CD20 Ab-mPEG scFv) and actively attracting PEGylated liposomal doxorubicin to enhance anti-tumor activity. J Nanobiotechnol 2021; 19:1-12.
14. Coiffier B, Lepretre S, Pedersen LM, Gadeberg O, Fredriksen H, van Oers MH, *et al.* Safety and efficacy of ofatumumab, a fully human monoclonal anti-CD20 antibody, in patients with relapsed or refractory B-cell chronic lymphocytic leukemia: A phase 1-2 study. Blood 2008; 111:1094-1100.
15. Barth MJ, Czuczman MS. Ofatumumab: a novel, fully human anti-CD20 monoclonal antibody for the treatment of chronic lymphocytic leukemia. Future Oncol 2013; 9:1829-1839.
16. Maleki R, Rahimpour A, Rajabibazl M. Construction and evaluation of wild and mutant ofatumumab scFvs against the human CD20 antigen. Prep Biochem Biotechnol 2023; 53:239-246.
17. Andrade Â, Ferreira R, Fabris J, Domingues R. Coating nanomagnetic particles for biomedical applications. BME frontiers 2011:157-176.
18. Zhao Y, Zhao X, Cheng Y, Guo X, Yuan W. Iron oxide nanoparticles-based vaccine delivery for cancer treatment. Mol Pharm 2018; 15:1791-1799.
19. Kim EH, Lee HS, Kwak BK, Kim B-K. Synthesis of ferrofluid with magnetic nanoparticles by sonochemical method for MRI contrast agent. J Magn Magn Mater 2005; 289:328-330.
20. Luktuke S, Raj A, Santra S, Das S, Chakravorty A, Ramesh K, *et al.* Interaction of Fe_2O_3 and Fe_3O_4 Nanoparticle with Pathogenic Bacteria: A *in-silico* molecular mechanism study. J Nanosci Nanotechnol 2024; 14:40-48.
21. Sæbø IP, Bjørås M, Franzyk H, Helgesen E, Booth JA. Optimization of the hemolysis assay for the assessment of cytotoxicity. Int J Mol Sci 2023; 24:2914.
22.Van Meerloo J, Kaspers GJ, Cloos J. Cell sensitivity assays: The MTT assay. Cancer cell culture: Methods and protocols: Springer; 2011. p. 237-245.
23. Jain TK, Morales MA, Sahoo SK, Leslie-Pelecky DL, Labhasetwar V. Iron oxide nanoparticles for sustained delivery of anticancer agents. Mol Pharmaceutics 2005; 2:194-205.
24. Gupta AK, Gupta M. Synthesis and surface engineering of iron oxide nanoparticles for biomedical applications. Biomaterials 2005; 26:3995-4021.
25. Jumper J, Evans R, Pritzel A, Green T, Figurnov M, Ronneberger O, *et al.* Highly accurate protein structure prediction with AlphaFold. nature 2021; 596:583-589.
26. Varadi M, Anyango S, Deshpande M, Nair S, Natassia C, Yordanova G, *et al.* AlphaFold protein structure database: Massively expanding the structural coverage of protein-sequence space with high-accuracy models. Nucl Acids Res 2022; 50:D439-D444.
27. Laurent S, Forge D, Port M, Roch A, Robic C, Vander Elst L, *et al.* Magnetic iron oxide nanoparticles: Synthesis, stabilization, vectorization, physicochemical characterizations, and biological applications. Chem Rev 2008; 108:2064-2110.
28. Mahmoudi M, Sant S, Wang B, Laurent S, Sen T. Superparamagnetic iron oxide nanoparticles (SPIONs): development, surface modification and applications in chemotherapy. Adv Drug Deliv Rev 2011; 63:24-46.
29. Winiarczyk K, Gac W, Cioral-Kowalczyk M, Surowiec Z. Magnetic properties of iron oxide nanoparticles with a DMSA-modified surface. Hyperfine Interactions 2021; 242:48.
30. Jiang S, Wang X, Zhang Z, Sun L, Pu Y, Yao H, *et al.* CD20 monoclonal antibody-targeted nanoscale drug delivery system for doxorubicin chemotherapy: An *in vitro* study of cell lysis of CD20-positive Raji cells. Int J Nanomedicine 2016:5505-5518.
31. Huang X, Yi C, Fan Y, Zhang Y, Zhao L, Liang Z, *et al.* Magnetic Fe_3O_4 nanoparticles grafted with single-chain antibody (scFv) and docetaxel loaded β-cyclodextrin potential for ovarian cancer dual-targeting therapy. Mater Sci Eng: C 2014; 42:325-332.
32. Naeri A, Osouli M. EGFR targeted nanocarriers for cancer diagnosis and therapy. Trends Pept Protein Sci 2017; 1:41-55.